Pixel-Level Calibration in the Kepler Science Operations Center Pipeline

Elisa V. Quintana[*a], Jon M. Jenkins[a], Bruce D. Clarke[a], Hema Chandrasekaran[b], Joseph D. Twicken[a], Sean D. McCauliff[c], Miles T Cote[d], Todd C. Klaus[c], Christopher Allen[c], Douglas A. Caldwell[a], Stephen T. Bryson[d]

[a]SETI Institute, 515 N. Whisman Road, Mountain View, CA USA 94043;
[b]Lawrence Livermore National Laboratory, P.O. Box 808, L-478, Livermore, CA, USA 94551;
[c]Orbital Sciences Corporation, MS 244-30, Moffett Field, CA, USA 94035;
[d]NASA Ames Research Center, MS 244-30, Moffett Field, CA, USA 94035

ABSTRACT

We present an overview of the pixel-level calibration of flight data from the *Kepler Mission* performed within the Kepler Science Operations Center Science Processing Pipeline. This article describes the calibration (CAL) module, which operates on original spacecraft data obtained from the Data Management Center to remove instrument effects and other artifacts that pollute the data. CAL performs traditional CCD data reduction (removal of instrument/detector effects such as bias and dark current), pixel-level calibration (correcting for cosmic ray hits and variations in pixel sensitivity), *Kepler*-specific corrections (smear signals which result from the lack of a shutter on the photometer and distortions from the readout electronics), and additional operations that are needed due to the complexity and large volume of flight data. CAL operates on long (~30 min) and short (~1 min) sampled data, as well as full-frame images, and produces calibrated pixel flux time series, uncertainties, and other metrics that are used in subsequent Pipeline modules. The raw and calibrated data are also archived in the Multi-mission Archive at Space Telescope at the Space Telescope Science Institute for use by the astronomical community.

Keywords: *Kepler*, Space Telescope, Transit Photometry, Calibration

1. INTRODUCTION

The primary goal of the *Kepler Mission* is to detect Earth-size planets transiting Sun-like stars outside of the Solar System. In order to obtain the precision needed to detect such small photometric signals, the flight data is subject to numerous data processing steps that are performed in a complex automated pipeline which was developed in the Kepler Science Operations Center (SOC). The SOC Science Processing Pipeline[1,2] (hereafter referred to as the Pipeline) is composed of a number of modules that operate sequentially, including calibration (CAL), photometric analysis[3] (PA), pre-search data conditioning[4] (PDC), transiting planet search[5] (TPS), and data validation[6] (DV). Additional modules operate in parallel to monitor the instrument performance[7,8] and provide target management[9]. The flight data are processed monthly and quarterly[10], and are subject to continuous reprocessing throughout the length of the mission as the Pipeline algorithms continue to improve. Once each data set is processed through the Pipeline, the SOC provides a list of planetary candidates to the Science Team for further analysis.

Herein, we describe the first component of the Pipeline, CAL, which processes original flight pixel data provided by the Data Management Center at the Space Telescope Science Institute (STScI). Various data types are collected and differ by the number of integrations that compose each sampling time (or "cadence"), and also by the number and location of pixels that are collected. The raw data include photometric (target and background) pixels, along with a subset of the CCD termed "collateral data" which includes masked and over-clocked rows and columns that are used primarily for calibration. Three types of data sets are processed within CAL: (1) select pixels from >150,000 long cadence (LC)

[*]elisa.quintana@nasa.gov; phone 1 650 604 2467; fax 650-604-2478

targets that are collected every 29.4 minutes (with 270 exposures per cadence); (2) a smaller set of pixels from 512 short cadence (SC) targets that are sampled more frequently at 0.98 minute intervals (with 9 exposures per cadence); and (3) full-frame image (FFI) data which contain all available pixels for a single long cadence. These data types are processed separately in the Pipeline, and the differences will be noted herein.

This article describes the data flow within CAL and the methodology and reasoning behind the individual corrections that are applied to the different pixel types. Many of the primary corrections use external models[11] of each CCD that were developed from pre-flight hardware tests and FFI data taken during commissioning[12] (prior to the dust cover ejection). We discuss how these models are applied within CAL to correct for 2D bias structure, gain and nonlinearity of the conversion from analog-to-digital units (ADU) to photoelectrons, local detector electronics effects (undershoot and overshoot), and flat field (variations in pixel sensitivity). Other artifacts that need to be removed include excess charge from saturated stars that leak into the masked and virtual regions, cosmic ray events, dark current and smear. Note that CAL does not include any time or motion corrections or coordinate transformations. We present an overview of the focal plane CCD components and the pixels that are calibrated in the next section. Section 3 describes the individual calibration steps, presented in the order that they are performed, along with the additional functionalities of CAL. In Section 4, we present a summary of the CAL module and discuss future work that will help to improve the quality of the data.

2. KEPLER DATA FORMATS

The *Kepler* focal plane is composed of 42 charge-coupled device (CCD) cameras (Figure 1). A CCD "module" refers to a pair of CCDs that share a field flattener and are read out simultaneously by the detector electronics. Each of the 21 modules is composed of four CCD "outputs" that are each read out by a separate analog signal chain. The module integers range from [2-4, 6-20, 22-24], and the output integers range from [1-4]. Four fine guidance sensors (FGSs) on the corners of the focal plane (modules [1, 5, 23, 25], not shown in Figure 1) collect pointing information rather than science data and are not processed in the Pipeline. There are therefore 84 CCD "channels" that can be mapped to a unique module/output (ex. channel 19 = module/output 7/3). The CAL software component operates on a single CCD channel at a time.

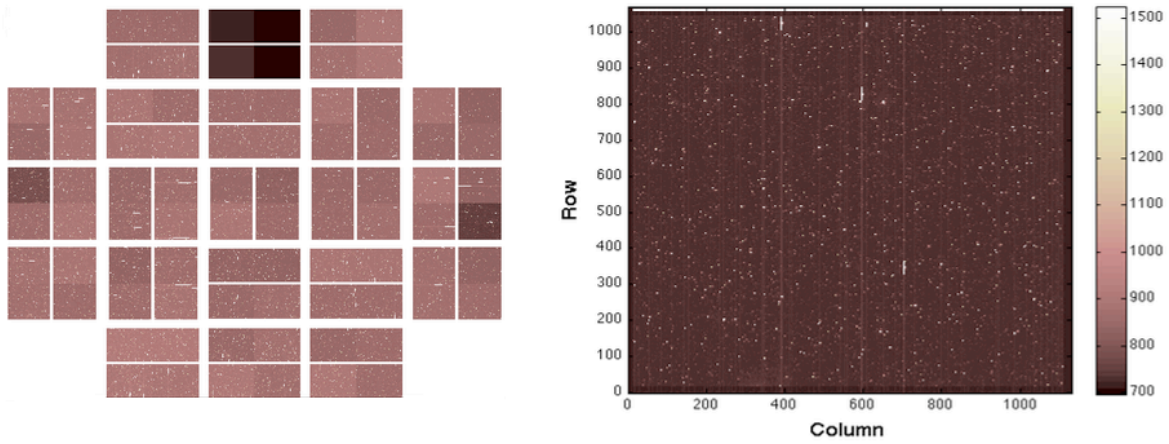

Figure 1. An uncalibrated image of the *Kepler* focal plane array (left panel) shows the 42 science CCDs, each of which is composed of two channels. Note that module 3 (the dark-colored module) is no longer working as of January 2010. An uncalibrated full-frame image (right panel) is shown for a single channel (19) from Quarter 4 Month 1 flight data (the pixel flux is in units of ADU per cadence).

2.1 Pixel Collection

Each CCD channel consists of an array of pixels with 1070 rows and 1132 columns, of which only a subset (1024 x 1100) is photometric (Figure 2). The full (1070 x 1132) array of pixels is downlinked for FFI data, whereas only select

target and background pixels are downlinked for LC and SC data due to limitations in memory, bandwidth, and the design of the flight software[9]. For LC, an upper limit of 170,000 stellar targets and 1125 background targets are collected across the focal plane (with additional limitations on the number per channel and the total pixel count). In addition, LC collateral data (black, masked smear, and virtual smear pixels, which are described in the next section) are collected for all rows and columns. For SC, a maximum of 512 stellar targets across the focal plane are collected, along with a subset of the collateral pixels: the black rows and smear columns that lie in the projection of photometric pixels onto the collateral region (Figure 2). Because smear pixels need to be corrected for the black level, the black pixels that lie in the projection of the masked and virtual smear pixels are also collected.

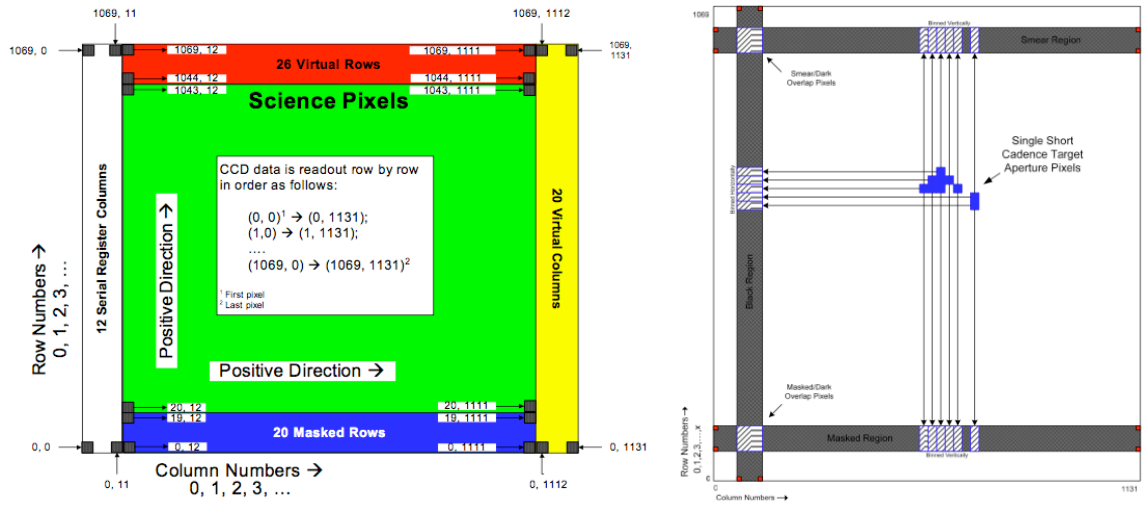

Figure 2. A schematic of the pixel types in a single CCD channel. The left panel shows the location of photometric pixels, along with the collateral pixels on the perimeter of the CCD. Only a subset of black columns and smear rows are collected and co-added onboard the spacecraft. For LC data, all black rows and smear columns are collected, whereas for SC (right panel) only collateral data in the projection of pixels (shaded regions) are collected.

2.2 Photometric and Collateral Data

The photometric pixels include all available target and background pixels on a CCD channel. In PA (the Pipeline module that follows CAL), the photometric pixels are packaged into individual stellar and background targets to create target flux time series. Within CAL, however, the target and background pixels are indistinguishable and the calibration steps are processed on the individual pixels.

The collateral data consist of a subset of the total available collateral, which includes the following: (1) 12 LC "leading black" pixels that represent virtual (non-physical) pixels, which are read out before the photometric pixels in each row; (2) 20 LC "trailing black" pixels, which are read out after the photometric pixels in each row; (3) 20 LC "masked smear" pixels, which are physical pixels closest to the serial register that are covered with an opaque aluminum mask; and (4) 26 LC "virtual smear" pixels, which are read out after all of the photometric pixels are clocked out. Only a subset of the trailing black (currently columns 1119-1132) is used for calibration, values which are set by the ground segment in a spacecraft configuration map that is uplinked to the spacecraft. The pixels in each row are co-added onboard the spacecraft prior to downlink, therefore each 'black pixel' is essentially the sum of 14 black pixel values per cadence. Likewise, a subset of masked (rows 7-18) and virtual (rows 1047-1058) is used for the co-added 12 masked and 12 virtual smear pixels per cadence. For SC data only, the cross-sections of trailing black columns and masked smear rows yield the "masked black" pixels, and the overlap of virtual rows and black columns gives the "virtual black" pixels (each of which is a scalar value equal to the sum of the number of black pixels times the number of smear pixels, or 14*12 = 168 co-adds per cadence). For FFI data, CAL uses the spacecraft configuration map to determine which collateral pixels should be used in calibration, and the data is processed as if it were a single LC.

2.3 Processing order

Data for each CCD channel are calibrated individually. Regardless of cadence type, the collateral pixels are always processed first to estimate the bias, smear, and dark levels. The photometric pixel calibration follows, using results calculated from the collateral data output. For FFIs, the collateral regions are processed first to obtain the black, smear, and dark level estimates, and then the entire array (collateral plus photometric) is calibrated using these values.

2.4 Data Gaps

All pixel data is accompanied by logical arrays (the same size as the pixel arrays) of spatial and temporal gaps, and only the available pixels are calibrated. In some calibration steps, such as the black and dark level estimation, CAL interpolates across missing cadences. The only cases for which data may be gapped *within* CAL include (1) cadences that occur during a momentum dump, (2) cadences that occur when the spacecraft is not in fine point (when the spacecraft attitude is not precisely controlled by the fine guidance sensors[12]), and (3) masked or virtual columns that have excess flux due to saturated stars that bleed into those columns.

3. CALIBRATION

A schematic of the data flow in the CAL module is shown in Figure 3, and the primary calibration steps are described here. All cadence types (FFI, LC, and SC) and pixel types (collateral and photometric) are processed separately, but use the same code base (with the exceptions noted in this section). For each cadence type and channel, the first invocation processes collateral (black and smear) pixels for all cadences. The outputs to this first pass include calibrated black and smear pixels, collateral and comic ray metrics, and more importantly the estimates for black, smear, and dark current for the specific channel that are needed to calibrate the photometric pixels. Due to the large volume of data, the photometric pixels array is subdivided by rows for LC processing, since the undershoot correction requires knowledge of all pixels in a row. For SC data, there are typically only 2-5 SC targets on a given channel but far more (30x) cadences than LC data, so we divide the pixels into cadence chunks. The boxes in Figure 3 with dashed lines show the steps that can be disabled in the Pipeline if desired.

3.1 Models

Some of the calibration steps rely on external models that characterize each CCD. These focal plane characteristics (FC) models[11] were developed during extensive ground-based tests, were updated in flight while the spacecraft dust cover was still in place, and are continuously monitored by the FC Pipeline module. These time-dependent models include (1) a read noise model, which gives the read noise per channel; (2) a 2D black model, which provides a 2D map of the black/bias structure per channel; (3) a gain model, which gives the ADU-to-photoelectrons conversion factor per channel; (4) a linearity model, which provides a set of polynomial coefficients used to correct for any nonlinearity in the gain transfer function; (5) an undershoot model, which includes filter coefficients that are used to correct for undershoot/overshoot artifacts caused by the CCD local detector electronics (LDE); and (6) a flat field model consisting of a 2D map of values that are used to correct for pixel sensitivity to a uniform light.

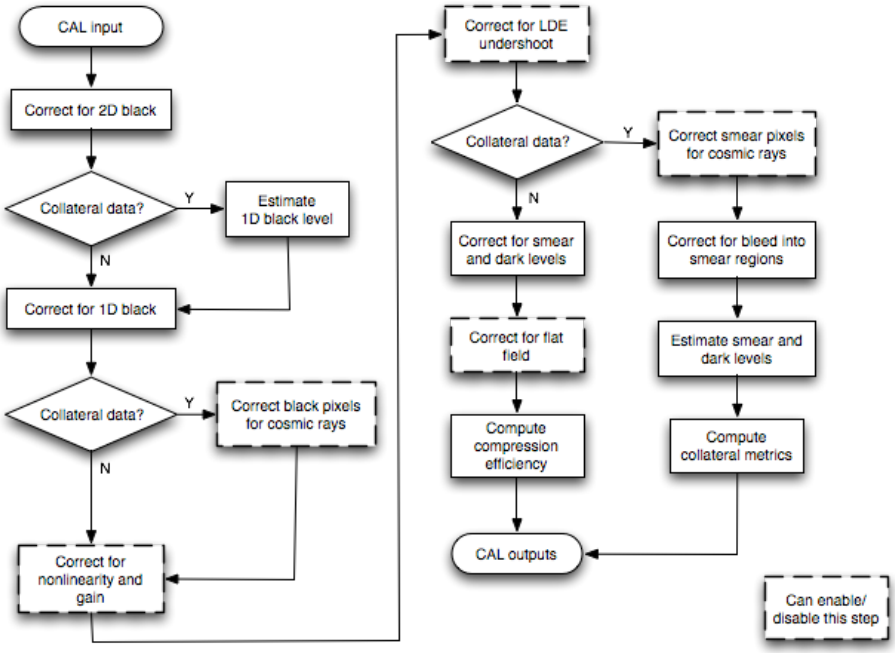

Figure 3. Data flow for calibrating collateral and photometric pixels. Dashed boxes indicate corrections that can be disabled in the Pipeline.

For the following calibration steps, the pixels that are corrected in each step will be denoted by $pixels_{COLL}$ (collateral) or $pixels_{PHOT}$ (photometric) if the correction only applies to that data type. If no subscript appears, the correction applies to all pixels.

3.2 Fixed Offset, Mean Black, and Spatial Coadds

Before the pixels are calibrated for black (bias) level, they are corrected for a "fixed offset" and "mean black" value. These values (which vary for SC and LC and across channels) were introduced to deal with spatial variations in bias and gain across the focal plane array, and to address issues with the pixel requantization scheme. Prior to downlink, all pixels are subject to requantization in which each pixel value is mapped to a discrete value in a pre-generated requantization table in order to control the quantization noise (the round-off error resulting from digitizing the voltage signals) to within ¼ of the intrinsic measurement uncertainty. Because collateral pixels are spatially coadded and fall on a different part of the requantization table, the mean black and fixed offset work by adjusting all channels to a common zero point to ensure proper requantization:

$$pixels = pixels - (fixed\ offset) + (mean\ black)$$

The original photometric pixels are in units of ADU/cadence. As described above, the collateral pixels are each the sum of a set of pixels and are normalized prior to calibration:

$$pixels_{COLL} = pixels_{COLL} / n_{coadds}$$

where n_{coadds} is the number of spatial coadds. At this point, all pixels are in units of ADU/cadence.

3.3 Black Correction

The black level correction includes 2D and 1D black corrections, in addition to cosmic ray detection in the black pixels. The "black level" refers to the bias in each CCD channel, and is an electronic offset that has been added to the CCD

voltage to ensure that positive signals are input into the analog-to-digital converter (ADC). The bias has a 2D structure that is characterized for each channel in a 2D black model, which was developed during ground testing of the CCD and with reverse-clocked images (which omit starlight). Some causes of the image artifacts include heating of the readout electronics, start of line (SOL) transients, parallel frame transfer signals, and FGS crosstalk clocking signals that are injected into the photometric region as the image is read out. Figure 4 shows an example of a 2D black model (left panel), and a close-up (right panel), that clearly shows the frame transfer and crosstalk features that must be removed from the science pixels. The 2D black model (in ADU/exposure) is extracted within CAL for each cadence for the appropriate pixels and simply subtracted off:

$$\text{pixels} = \text{pixels} - (\text{2D black} * n_{exp})$$

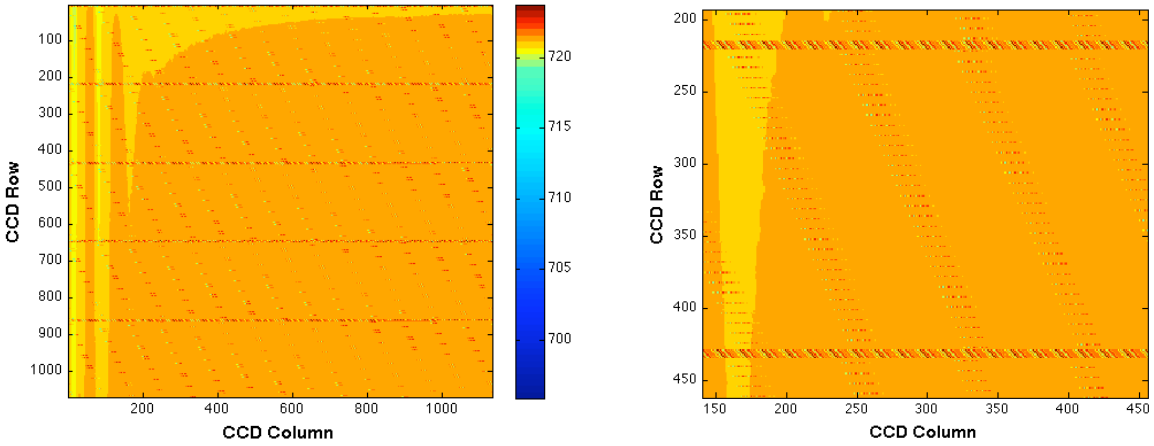

Figure 4. An example of a 2D black model (values in ADU/exposure), and a close-up (right panel), that clearly shows a 2D bias structure that needs to be removed from the science pixels.

where n_{exp} is the number of exposures per cadence. Once the 2D black level is removed, a fit to the residual bias is used to estimate a 1D black correction. The polynomial model order for the best fit is determined in an iterative fashion using the Modified Akaike Information Criterion[13] (MAIC). A robust fit is first performed to protect from outliers (neglecting the charge injection rows), and a least squares with known covariance method is used with the computed best polynomial order to produce the fit, or "black correction". This black correction is subtracted from the pixels:

$$\text{pixels} = \text{pixels} - (\text{black correction})$$

Following the 1D black correction, the black pixels are corrected for cosmic rays (if the cosmic ray flag is enabled) and saved for output, as they are no longer needed for calibration. Note that CAL only corrects LC and SC collateral pixels for cosmic rays, and uses the same methodology as the photometric pixel cosmic ray correction that is performed within PA[3].

3.4 Nonlinearity and Gain Correction

The gain and nonlinearity describe the transfer function from photoelectrons (e-) in the CCD to ADU coming out of the ADC. Linearity is a measure of the deviation from the linear transfer function at each ADU signal level. The nonlinearity model provides polynomial coefficients for each exposure, so the nonlinearity correction can be estimated by evaluating the polynomial (P) at the black-corrected pixel values (normalized by the number of exposures). If the nonlinearity flag is enabled, the pixels are corrected by:

$$\text{pixels} = \text{pixels} * P(\text{pixels}/n_{exp}) * n_{exp}$$

Gain is the average slope of the transfer function, and has a median value of 112 e-/ADU across the focal plane[14]. The gain model provides the gain (scalar) value per channel per cadence in e-/ADU, and all pixels are converted to e-/cadence by:

$$\text{pixels} = \text{pixels} * \text{gain}$$

3.5 LDE Undershoot Correction

Overshoot and undershoot are distortions in the signal that result from operating the clamp circuit in the local detector electronics with insufficient bandwidth. The impulse response artifacts are most noticeable after light-to-dark (undershoot) and dark-to-light (overshoot) transitions, and clearly show spikes in the pixel row time series of targets affected by this artifact (Figure 5). Ground-based tests demonstrated that these artifacts can be modeled as a linear shift-invariant (LSI) distortion, and the undershoot model provides a set of filter coefficients for each channel and cadence. If the undershoot flag is enabled in the Pipeline, data is interpolated across rows to fill in missing pixels, and a linear digital filter (F) is applied to each row to correct for the undershoot/overshoot:

$$\text{pixels} = F(\text{coefficients}, \text{pixels})$$

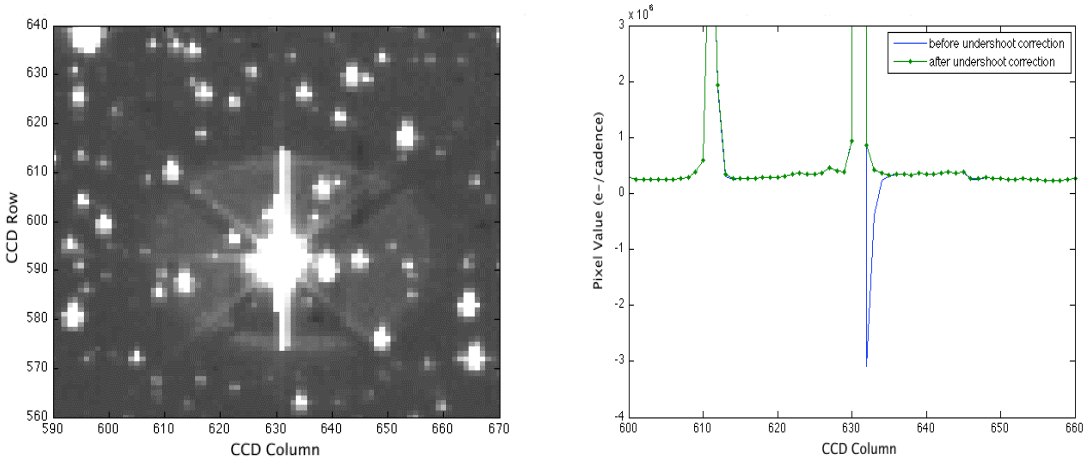

Figure 5 An example of a bright target star (left panel), and the undershoot response (the negative spike in the right panel) for row 611, along with the corrected pixel values.

If the cosmic ray flag is enabled, the LC and SC masked and virtual smear pixels are corrected for cosmic rays and saved for output. The masked/virtual smear pixels are still used to estimate the smear and dark current levels that are needed to correct the photometric pixels (as described in the next section), but the "calibrated smear" pixels that are output to the Multi-mission Archive at Space Telescope (MAST) at STScI consist of the calibrated pixels up to this point.

3.6 Smear and Dark Correction

The target and background pixels are also corrected for smear and dark current levels. The *Kepler* photometer is operated without a shutter, so stars smear along columns as the CCD is read out and are clearly visible in FFI data (Figure 6). Dark current is a thermally induced signal in each physical pixel during an integration period, which includes the exposure time (t_{exp} ~ 6.02 s) and readout time (t_{read} ~ 0.52 s). These corrections are grouped together because the smear and the dark levels can be estimated from linear combinations of the virtual and masked smear pixels.

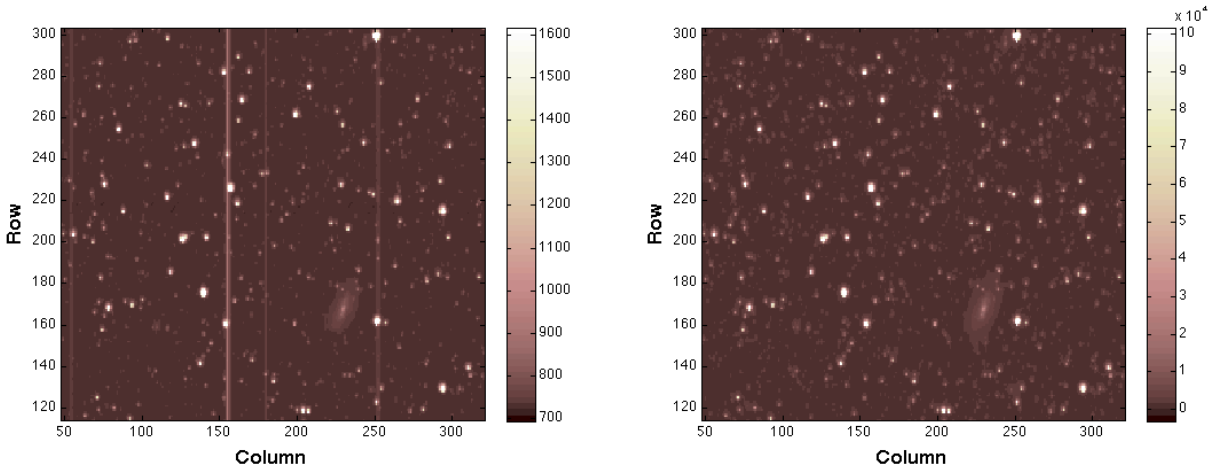

Figure 6 A portion of an uncalibrated FFI (in units of ADU/cadence, left panel) and the calibrated image (in photoelectrons/cadence, right panel) demonstrate the removal of smear.

The masked smear pixels, which are shielded from star flux, detect dark current during an integration and collect the smear signal from the photometric and over-clocked virtual pixels during readout. The virtual pixels only contain dark current that is accumulated during readout time, but collect smear as they are clocked through the image. The dark current (e-/pixel/sec) can be computed by:

$$\text{dark current} = (\text{masked} - \text{virtual}) / (n_{exp} * t_{exp})$$

The dark level (e-/pixel) is computed as the average of the difference between the valid masked and virtual measurements in each column:

$$\text{dark level} = (\text{dark current}) * n_{exp} * (t_{exp} + t_{read})$$

We also interpolate dark level values over missing cadences to ensure that a dark level is available for all cadences. To compute the smear level, the dark level is first removed from the masked and virtual pixels. Ideally, both masked and virtual pixels would be available for each column and for all cadences. If either is unavailable for a particular column, then the available smear pixel value is used. If neither is available, the smear correction cannot be performed for the entire column. We use the logical gap indicator arrays that are provided with the pixel arrays to estimate the smear as follows:

$$\text{masked pixels} = (\text{masked} - \text{dark level}) * (\text{valid masked})$$

$$\text{virtual pixels} = (\text{virtual} - \text{dark level}) * t_{read} / (t_{exp} + t_{read}) * (\text{valid virtual})$$

where (valid masked) and (valid virtual) represent logical gap arrays where gaps = true. The smear in each column is then estimated using the following logic:

Available Masked	Available Virtual	C_{Masked}	$C_{virtual}$
True	True	1/2	1/2
True	False	1	0
False	True	0	1
False	False	0	0

where C_{Masked} and $C_{virtual}$ are coefficients in the linear combination of the dark-corrected masked and virtual smear pixels:

$$C_{Masked} = 1/2 * (\text{valid masked}) * (1 + \text{gapped virtual})$$

$$C_{Virtual} = 1/2 * (\text{valid virtual}) * (1 + \text{gapped masked})$$

$$\text{smear level} = \text{masked} * C_{\text{Masked}} + \text{virtual} * C_{\text{Virtual}}$$

The above smear and dark level estimates are computed during the collateral data calibration, resulting in a mean dark level value per CCD channel and an array of smear levels per column per channel. These are later subtracted from the photometric pixels by column:

$$\text{pixels}_{\text{PHOT}} = \text{pixels}_{\text{PHOT}} - (\text{dark level}) - (\text{smear level})$$

An additional complication to the smear level estimate is bleeding charge from saturated targets into the masked or virtual smear regions that are clearly visible in FFI data. CAL detects and gaps columns that are corrupted by bleeding charge in LC masked or virtual smear data, but currently does not search for bleeding charge in short cadence data.

3.7 Flat Field Correction

The flat field is the final major calibration step, and operates on photometric pixels to correct for spatial and temporal variations in pixel sensitivity to a uniform light source. Differences in pixel response can be due to variations in quantum efficiency or throughput changes in the field flattener lenses or anti-reflection coating of the CCD[14]. The flat field model includes a large-scale (where spatial regions are large compared to a pixel) and small-scale (pixel-to-pixel) flat field map. Only the small-scale flat field is needed for CAL, and the values represent the percent deviation from the local mean. If the flat field flag is enabled, the flat field 2D model is divided from the appropriate photometric pixels for each cadence:

$$\text{pixels}_{\text{PHOT}} = \text{pixels}_{\text{PHOT}} / (\text{flat field})$$

3.8 Additional Functionality in CAL

At the end of the last invocation of CAL for each CCD channel, the theoretical and achieved compression efficiency of the data is computed. These metrics, along with time series of black, smear, and dark level metrics also computed within CAL, are used by the photometer performance assessment (PPA)[8] module to track and trend the data. CAL also has the capability to propagate uncertainties in a separate propagation of uncertainties (POU) module[15]. The primary noise sources for *Kepler* include read noise, which is an additive noise source due to the readout process, quantization noise that is stochastic and results from quantization in the analog-to-digital converter and pixel requantization, and Poisson-like shot noise. The uncertainties in the raw pixel data are computed at the start of CAL, and (if enabled) POU runs in parallel with CAL and the uncertainties are propagated at each transformation step. If POU is disabled, then the outputs to CAL are the raw uncertainties corrected only for gain.

4. SUMMARY AND FUTURE WORK

We have described the pixel-level corrections that are performed in the CAL Pipeline for LC, SC, and FFI flight data. The data corrections include: 2D and 1D bias, gain, nonlinearity, undershoot and overshoot distortions from the LDE electronics, cosmic rays, bleeding charge, dark current, smear due to the lack of a shutter on the instrument, and flat field variations. The algorithms were validated using simulated flight data from the End-To-End-Model[16] (ETEM) that was developed in the SOC, which simulates every layer of the data – from CCD and instrument artifacts to transit light curves – and has proven to be a powerful tool in the development and testing of the Pipeline modules. Output from CAL that is exported to the MAST includes raw and calibrated black, smear, and photometric pixels, along with the associated gap indicators and uncertainties. Additional metrics for cosmic ray detection, black level, smear level, and dark current level estimates are also provided.

Some issues that may be addressed in future versions of CAL include incorporating a more detailed time-varying 2D black model, refining the cosmic ray algorithms, and addressing bleeding charge in SC data. Due to the large volume of data that is processed each quarter (Q1, for example, yielded ~2TB for LC and SC CAL output alone), and the fact that the SOC will be reprocessing data throughout the duration of the mission, improving the performance of the algorithms is a high priority in order to maintain reasonable data processing times.

CAL has been successful at calibrating the flight data to high standards[14]. With data from just the first 10 days of flight, the *Kepler Mission* has detected and confirmed eight giant extrasolar planets to date[17] (including three that were known to exist in the *Kepler* field of view). The CAL algorithms and performance will continue to improve throughout the lifetime of the mission to support the search for smaller Earth-size planets.

ACKNOWLEDGEMENTS

The authors would like to thank Bill Borucki and Dave Koch for their decades-long dedication to *Kepler*, and the many others that contributed to the success of the mission. Special thanks to Sue Blumenberg for help with the preparation of the manuscript. Funding for the *Kepler* mission is provided by the NASA Science Mission Directorate.

REFERENCES

[1] Jenkins, J. M., *et al*., "Overview of the *Kepler* science processing pipeline," *ApJL* **713(2)**, L87–L91 (2010).
[2] Middour, C., *et al.*, "*Kepler* Science Operations Center architecture," *Proc. SPIE* **7740**, in press (2010).
[3] Twicken, J. D., *et al.*, "Photometric analysis in the *Kepler* Science Operations Center pipeline," *Proc. SPIE* **7740**, in press (2010).
[4] Twicken, J. D., *et al.*, "Presearch data conditioning in the *Kepler* Science Operations Center pipeline," *Proc. SPIE* **7740**, in press (2010).
[5] Jenkins, J. M., *et al.*, "Transiting planet search in the *Kepler* pipeline," *Proc. SPIE* **7740**, in press (2010).
[6] Wu, H., *et al*., "Data validation in the *Kepler* Science Operations Center pipeline," *Proc. SPIE* **7740**, in press (2010).
[7] Chandrasekaran, H., *et al.*, "Semi-weekly monitoring of the performance and attitude of *Kepler* using a sparse set of targets," *Proc. SPIE* **7740**, in press (2010).
[8] Li, J., *et al.*, "Photometer performance assessment in *Kepler* science data processing", *Proc. SPIE* **7740**, in press (2010)
[9] Bryson, S. T., *et al.*, "Selecting pixels for *Kepler* downlink," *Proc. SPIE* **7740**, in press (2010).
[10] Hall, J. R., *et al.*, "*Kepler* science operations processes, procedures, and tools," *Proc. SPIE* **7737**, in press (2010).
[11] Allen, C. A., *et al.*, "Focal plane characterization," *Proc. SPIE* **7740**, in press (2010).
[12] Haas, M., *et al.*, "*Kepler* science operations," *ApJL* **713(2)**, L115–L119 (2010).
[13] Akaike, H., "A New Look at the Statistical Model Identification," *IEEE Transactions on Automatic Control*, **AC-19 (6)**, 716–723 (1974)
[14] Caldwell, D. A., *et al.*, "Instrument performance in *Kepler's* first months," *ApJL* **713(2)**, L92–L96 (2010).
[15] Clarke, B. D., *et al.*, "A framework for propagation of uncertainties in the *Kepler* data analysis pipeline", *Proc. SPIE* **7740**, in press (2010)
[16] Bryson, S. T., *et al.*, "The *Kepler* end-to-end model: creating high-fidelity simulations to test *Kepler* ground processing," *Proc. SPIE* **7738**, in press (2010).
[17] Borucki, W., *et al.*, "*Kepler* planet-detection mission: introduction and first results," *Science* **327**, 977–980 (2010).